Ultrafast Hydration Dynamics in Melittin Folding and Aggregation: Helix Formation and Tetramer Self-Assembly

Weihong Qiu, Luyuan Zhang, Ya-Ting Kao, Wenyun Lu,† Tanping Li, Jongjoo Kim, Gregory M. Sollenberger,‡ Lijuan Wang, and Dongping Zhong*

Departments of Physics, Chemistry, and Biochemistry, OSU Biophysics, Chemical Physics, and Biochemistry Programs, 191 West Woodruff Avenue, The Ohio State University, Columbus, Ohio 43210

Received: March 7, 2005; In Final Form: July 1, 2005

Melittin, an amphipathic peptide from honeybee venom, consists of 26 amino acid residues and adopts different conformations from a random coil, to an α-helix, and to a self-assembled tetramer under certain aqueous environments. We report here our systematic studies of the hydration dynamics in these conformations using single intrinsic tryptophan (W19) as a molecular probe. With femtosecond resolution, we observed the solvation dynamics occurring in 0.62 and 14.7 ps in a random-coiled primary structure. The former represents bulklike water motion, and the latter reflects surface-type hydration dynamics of proteins. As a comparison, a model tripeptide (KWK) was also studied. At a membrane−water interface, melittin folds into a secondary α-helical structure, and the interfacial water motion was found to take as long as 114 ps, indicating a well-ordered water structure along the membrane surface. In high-salt aqueous solution, the dielectric screening and ionic solvation promote the hydrophobic core collapse in melittin aggregation and facilitate the tetramer formation. This self-assembled tertiary structure is also stabilized by the strong hydrophilic interactions of charged C-terminal residues and associated ions with water molecules in the two assembled regions. The hydration dynamics was observed to occur in 87 ps, significantly slower than typical water relaxation at protein surfaces but similar to water motion at membrane interfaces. Thus, the observed time scale of ∼100 ps probably implies appropriate water mobility for mediating the formation of high-order structures of melittin in an α-helix and a self-assembled tetramer. These results elucidate the critical role of hydration dynamics in peptide conformational transitions and protein structural stability and integrity.

I. Introduction

Understanding protein−water interactions is fundamental to many aspects of protein behavior such as protein folding and aggregation, protein plasticity and recognition, and enzymatic catalysis.[1−10] The protein-associated water (biological water) in the hydration layer plays a critical role in structural stability, flexibility, and integrity. The dynamics of water motions directly affects protein conformational transitions such as from the denatured to folded state[11,12] or from the misfolded structure to the final protein aggregate.[13,14] Thus, elucidation of molecular mechanisms of these interactions is essential to the understanding of protein dynamics,[1,3,15] as well as practically important, for example, to better control early protein misfolding and aggregation that occurs in neurodegenerative diseases.[16,17] Here, we use a prototype peptide, melittin, to systematically examine the water dynamics from a random-coiled primary state, to a folded α-helical secondary structure, and to the final self-assembled tertiary tetramer.

Melittin, a peptide toxin found in honeybee venom and one of the most studied archetypes of membrane proteins,[18−21] consists of 26 amino acid residues (Figure 1). The first 20 residues are predominantly hydrophobic while the other 6 near the carboxyl terminus are hydrophilic under physiological conditions. This amphipathic property makes melittin soluble in aqueous solution as well as easily bound to membranes. It typically exists in a random-coiled configuration in water[22−24] but readily forms an α-helix in alcohol solvents[25−27] or through interactions with a membrane.[18−21,28−30] In aqueous solution of high ionic strength, high peptide concentration, or high pH, melittin can aggregate into a tetramer.[22−24,26,31,32] The X-ray crystallographic structure[33] of the melittin tetramer shows a twofold symmetric configuration with two almost stereochemically identical dimers; each one consists of two antiparallel aligned α-helical monomers (Figure 1).

Melittin has been extensively studied to understand the interactions of peptide with biological membranes. Self-assembly of α-helical melittin monomers is believed to be important in its lytic activity of membranes.[18−21] Its adaptability of different conformations has also made melittin an ideal model system for studies of protein folding.[32] A number of simulations have been carried out to examine the interactions of melittin with water and membrane.[34−38] The single tryptophan residue (W19) has been widely used as an optical probe to study conformational dynamics through measurements of its steady-state emission,[28,39−41] orientational anisotropy, and fluorescence lifetimes.[42−45] Recent studies have shown that intrinsic tryptophan is very sensitive to microenvironment polarity, and its time-resolved fluorescence emission (Stokes shift) directly probes local solvation dynamics.[1,46−48] In this report, we first studied water motion around tryptophan in a tripeptide Lys-

* To whom correspondence should be addressed. Tel: (614)292-3044. Fax: (614)292-7557. E-mail: dongping@mps.ohio-state.edu.

† Present address: Lewis-Sigler Institute for Integrative Genomics, Princeton University, Princeton, NJ 08544.

‡ REU student, Department of Physics, Western Illinois University, Macomb, IL 61455.

10.1021/jp0511754 CCC: $30.25
Published on Web 08/17/2005

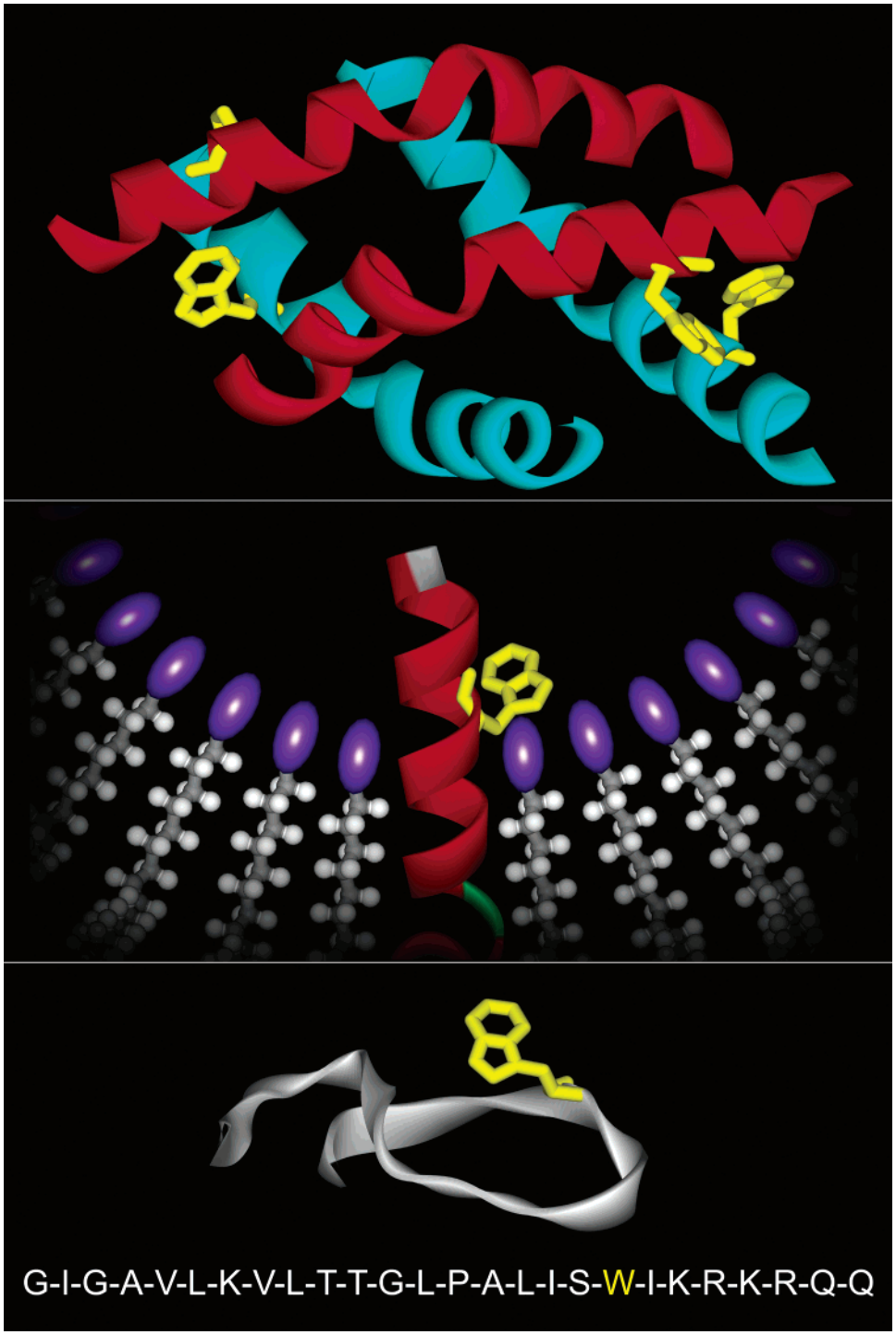

Figure 1. X-ray crystallographic structure of melittin tetramer (upper),[33] schematic illustration of membrane-bound α-helical melittin (middle), and melittin monomer in a random-coiled state (lower) from one trajectory MD simulation (800 ps) through melting of the α-helical monomer at 600 °C in water. Note that W19 in α-helical melittin is highly constrained at the membrane interface. The melittin sequence is given at the bottom.

Trp-Lys (KWK) with femtosecond (fs) resolution and then used intrinsic W19 to examine hydration dynamics in different conformations of melittin from a random coil, to a membrane-bound α-helix, and to a self-assembled tetramer in various aqueous solutions.

The paper is organized as follows. In section II, we describe the experimental methodology including our fs laser setup and sample preparation. In section III, we present the fs-resolved experimental results and discussion on hydration dynamics with different peptide conformations. Finally, the conclusion of our work is summarized in section IV.

II. Experimental Section

A. Femtosecond Laser Setup. All the fs-resolved measurements were carried out using a fluorescence up-conversion method. The integrated experimental setup has been described elsewhere.[49] Briefly, the fs pulse after the two-stage amplifier (Spitfire, Spectra-Physics) has a temporal width of 110 fs centered at 800 nm with an energy of more than 2 mJ/pulse and a repetition rate of 1 kHz. Half of the laser energy was used to pump an optical parametric amplifier (OPA-800C, Spectra-Physics) to generate signal (1289 nm) and idler (2109

nm) beams. The latter was mixed with the residual fundamental (800 nm) in a 0.2 mm thick β-barium borate crystal (BBO, type I) to generate a fs pulse at 580 nm. This fs pulse, compressed through a pair of prisms with double paths to reach a temporal resolution of 60 fs, was frequency doubled to generate our pump wavelength at 290 nm by another 0.2 mm thick BBO crystal. The pump pulse energy was typically attenuated to ~140 nJ prior to being focused into the motor-controlled rotating sample cell. The fluorescence emission was collected by a pair of parabolic mirrors and mixed with a gating pulse from another half of fundamental beam (attenuated) in a 0.2-mm BBO crystal through a noncollinear configuration. The up-converted signal ranging from 218 to 292 nm was detected by a photomultiplier coupled with a double-grating monochromator. The instrument response time under the current noncollinear geometry is between 400 and 500 fs as determined from the up-conversion signal of Raman scattering of water around 320 nm.

The pump-beam polarization was set at a magic angle (54.7°) with respect to the acceptance axis (vertical) of the up-conversion crystal, and the polarization of the gating beam was set parallel to this axis through a half-wave plate. For fluorescence anisotropy measurements, the pump-beam polarization was rotated either parallel or perpendicular to the acceptance axis to obtain the parallel ($I_{\parallel}$) and perpendicular ($I_{\perp}$) signals, respectively. These transients were used to construct time-resolved anisotropy: $r(t) = (I_{\parallel} - I_{\perp})/(I_{\parallel} + 2I_{\perp})$.

B. Sample Preparation. Both melittin and tripeptide-KWK were purchased from Sigma-Aldrich in lyophilized powder, Hepes chemicals from USB, lipid monoolein (1-oleoyl-rac-glycerol, >99% purity) from Nu Chek Prep (Elysian, MN), and all other chemical reagents from Fisher Scientific. All samples were used as received without further purification. Tripeptide-KWK was dissolved in Tris (100 mM) buffer solution at pH 7.5 with a concentration of 3 mM. Melittin was dissolved either in distilled water/HCl at pH 4 with a concentration of 1 mM to form a random-coiled monomer solution or in 100 mM Hepes/2 M NaCl at pH 7.5 with a concentration of 3 mM to reach a tetramer solution.[26,42] For membrane-bound melittin, the lipid−water mixture was made at 20 °C consisting of 60% (w/w) lipid monoolein and 40% (w/w) water solution which contains 2 mM melittin and 20 mM TES buffer at pH 7.4. Under these conditions, this mixture forms the lipidic cubic phase (*Pn*3*m*) with a diameter of aqueous channels at ~50 Å.[50]

C. Steady-State Fluorescence Characterization. The steady-state fluorescence spectra were characterized using a SPEX FluoroMax-3 spectrometer. The tryptophan fluorescence emission peaks at 349 nm in bulk water and shifts to 352 nm in 100 mM Tris buffer.[47] The emission of tripeptide-KWK has a maximum at 350.6 nm. Melittin in a random-coiled form exhibits an emission maximum at 348.5 nm, indicating a great exposure of intrinsic W19 to an aqueous environment. Upon incorporation into the lipidic cubic phase membrane, the emission peak shifts to 341 nm, suggesting a less polar microenvironment around W19 in the α-helical structure. The emission maximum of W19 upon tetramerization of melittin shifts further to the blue at 333.5 nm, consistent with a more hydrophobic location of W19 in the tetramer as observed by the X-ray structure.[33] These emission peaks of tryptophan in different conformations are well correlated with the degree of hydration of its local environments.

D. Construction of Solvation Correlation Function. The construction of solvent response function has been well studied using a single-lifetime dye molecule as an optical probe in solution.[51] Zhong and co-workers have demonstrated that such a conventional method is no longer applicable for the tryptophan probe because the fluorescence spectrum of excited tryptophan usually is a mixture of two emissions with two different lifetimes due to its inevitable ground-state heterogeneity (rotamers). An extended method has been recently introduced to construct a solvent response function using tryptophan as a solvation probe.[47]

Briefly, all fs-resolved fluorescence transients of tryptophan can be represented as a sum of two terms of discrete exponential functions

$$I_{\lambda}(t) = I_{\lambda}^{\mathrm{solv}}(t) + I_{\lambda}^{\mathrm{popul}}(t) = \sum_i \alpha_i e^{-t/\tau_i} + \sum_j \beta_j e^{-t/\tau_j} \quad \text{(II.1)}$$

where the first term associated with α_i and τ_i describes solvation processes, and the second term associated with β_j and τ_j represents intrinsic lifetime emissions (population decay). The coefficient α_i is positive (decay dynamics) at the blue side of the emission peak and is negative (initial rise) at the red side. The coefficient β_j is always positive and represents the relative contributions of lifetime emissions. Thus, the *overall* time-resolved emission spectra can be constructed as follows

$$I(\lambda,t) = \frac{I_{\lambda}^{\mathrm{ss}} I_{\lambda}(t)}{\sum_i \alpha_i \tau_i + \sum_j \beta_j \tau_j} \quad \text{(II.2)}$$

where $I_{\lambda}^{\mathrm{ss}}$ is the relative steady-state emission intensity at wavelength λ. The time-resolved spectrum, after being converted to intensity vs frequency in cm^{-1}, was fitted to a log-normal function to deduce the emission maximum $\nu_s(t)$. Thus, a function of emission maxima with time can be obtained. At a certain time (t_{sc}), solvation is complete and the emission maximum $\nu_s(t_{sc})$ should equal the *apparent* lifetime emission peak $\nu_l(t_{sc})$, which results from a mixture of two lifetime emissions and is constructed from a lifetime-associated time-dependent emission spectrum

$$I^{\mathrm{popul}}(\lambda,t) = \frac{I_{\lambda}^{\mathrm{ss}} I_{\lambda}^{\mathrm{popul}}(t)}{\sum_i \alpha_i \tau_i + \sum_j \beta_j \tau_j} \quad \text{(II.3)}$$

The emission maximum $\nu_l(t)$ is also deduced from a log-normal fit of the spectrum. For a convenience of further reference, we call τ_{sc} the solvation-complete time. Apparently, the emission maximum ν_{sc} at τ_{sc} differs from the steady-state emission peak ν_{ss}, and the solvation-complete time τ_{sc} is different from τ_{ss}, a time for the time-resolved spectrum to reach the steady-state emission. It is also readily realized that after solvation ends, the overall time-dependent emission peaks $\nu_s(t)$ merge into lifetime-associated emission maxima of $\nu_l(t)$. As a consequence of the fact that the lifetime-associated emission keeps moving to the red side with time, a more accurate method is to subtract the lifetime-associated emission contribution $\nu_l(t)$ from the overall emission maximum $\nu_s(t)$, and the solvent response function can be constructed as follows

$$c(t) = \frac{\nu_s(t) - \nu_l(t)}{\nu_s(0) - \nu_l(0)} \quad \text{(II.4)}$$

The constructed $c(t)$ function is finished at the time τ_{sc}, and this correlation function would be fitted to a multiple-exponential decay. Practically, we consider the time when the difference

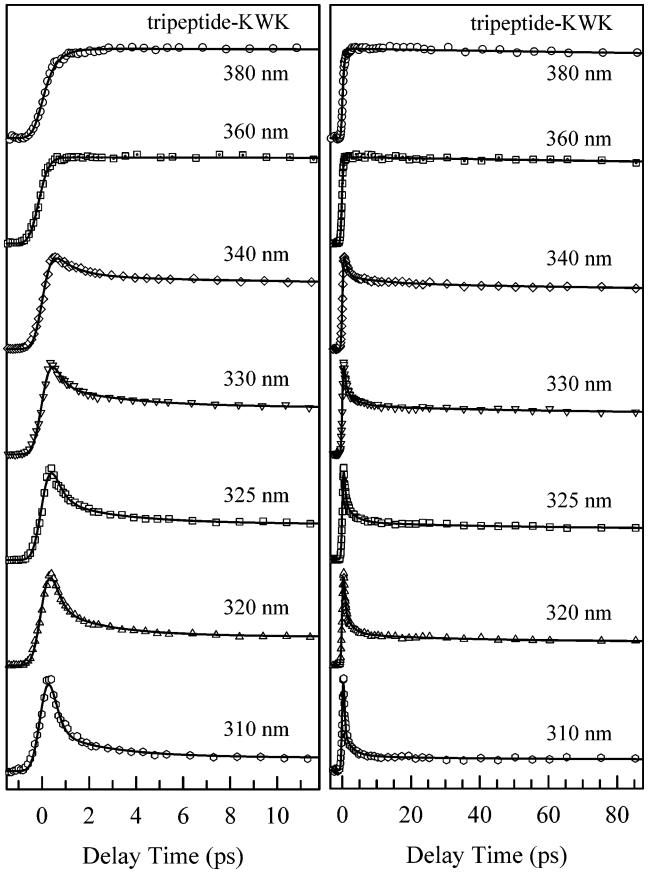

Figure 2. Normalized, fs-resolved fluorescence transients of tripeptide-KWK in the short (left) and long (right) time ranges with a series of gated fluorescence emissions.

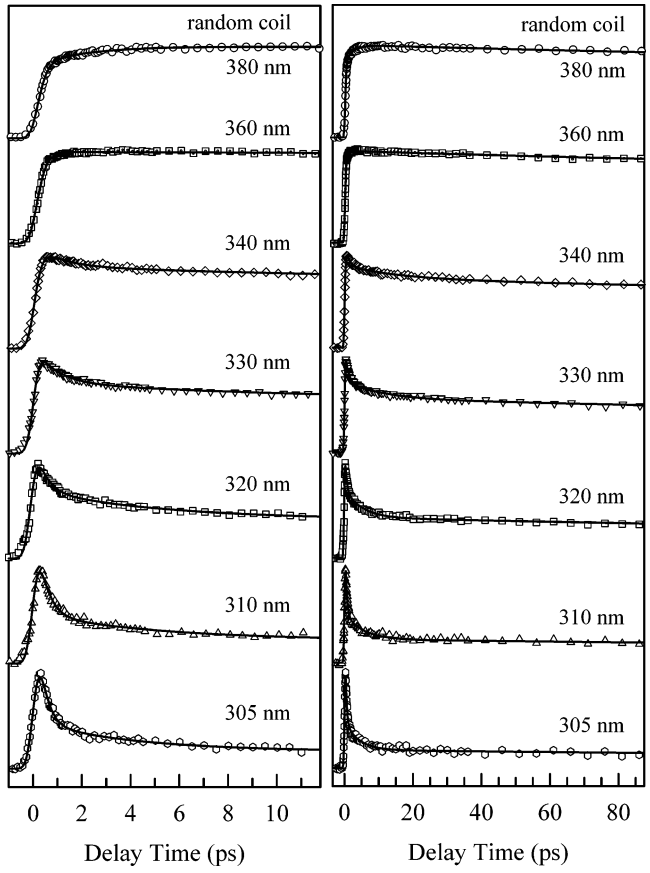

Figure 3. Normalized, fs-resolved fluorescence transients of a random-coiled melittin in water in the short (left) and long (right) time ranges with a series of gated fluorescence emissions.

between $\nu_s(t)$ and $\nu_l(t)$ is less than 0.5 cm^{-1} as the solvation-complete time τ_{sc}. For a molecular probe with only single-lifetime emission, $\nu_l(t) = \nu_l(0) = \nu(\infty)$ always holds because the lifetime-associated emission no longer varies with time and eq II.4 converges to the conventional one.[51] It should be noted that the difference between $\nu_{sc}(t_{sc})$ and $\nu_{ss}(t_{ss})$ purely results from the mixture of two lifetime emissions. The time evolution from ν_{sc} to ν_{ss} could be very long. Here, the steady-state emission maximum, obtained from an integration of all time-resolved spectra, is *not* relevant for the construction of the correlation function.

III. Results and Discussion

A. Femtosecond-Resolved Fluorescence Dynamics. A series of fs-resolved fluorescence up-conversion transients with different peptide conformations are shown in Figures 2−5 and more than ten emission wavelengths were gated from the blue to the red side for each conformation. A global fitting strategy was used to fit all the transients. Typically, four or five discrete exponential functions were used, and among these are two lifetime emission decays. The two fluorescence lifetimes (∼500 ps and ∼3 ns)[42] were fixed for all transients of each peptide structure.

(a) Tripeptide-KWK. Figure 2 shows fluorescence temporal behavior of tryptophan in tripeptide-KWK, and the overall decay dynamics is similar to that of tryptophan in the same buffer.[47] Besides the two lifetime contributions ($I_\lambda^{popul}(t)$), three exponential decays ($I_\lambda^{sol}(t)$) were used to represent the solvation dynamics. At the blue side, the three decays occur in 0.22−0.4, 1.8−3.4, and 8−24 ps, and the first ultrafast component dominates. At the red side (≥350 nm), an initial rise was observed in all transients within 0.2−0.5 ps followed by two lifetime emissions.

(b) Melittin: A Random Coil. Figure 3 shows a set of fs-resolved fluorescence transients of melittin monomer in water at pH 4 in a random-coiled form. At the blue side, the transients exhibit two solvation components. These components decay in 0.4−1.3 and 4.4−25 ps with considerable contributions, respectively. At the red side (≥350 nm), we observed two initial rise components in all transients with the time scales of 0.24 and 1.8−4.2 ps. Compared with the results of the tripeptide above, this random-coiled peptide shows overall slower solvation dynamics.

(c) Melittin: A Membrane-Bound α-Helix. Figure 4 shows a series of fs-resolved fluorescence transients of melittin at membrane−water interfaces. Compared with the transients of the random-coiled monomer in Figure 3, the solvation dynamics becomes drastically slower. At the blue side, three solvation components were observed and they decay in 0.6−4, 7−23, and 71−120 ps with similar amplitudes, respectively. At the red side (≥340 nm), we observed two initial rise components in 0.5 and 22 ps. Compared with those of free tryptophan in the same lipidic cubic phase,[47] the first solvation component observed here slows down but the other two longer components have similar dynamics.

(d) Melittin: A Self-Assembled Tetramer. We studied the solvation dynamics of melittin aggregation to tetramer formation under high-salt conditions. Because of its symmetry (Figure 1), all four tryptophan residues in the tetramer nearly have the same microenvironments. Figure 5 shows the fluorescence temporal behavior in the tetramer conformation. Similar to the membrane-bound α-helix in Figure 4, we observed significantly slow

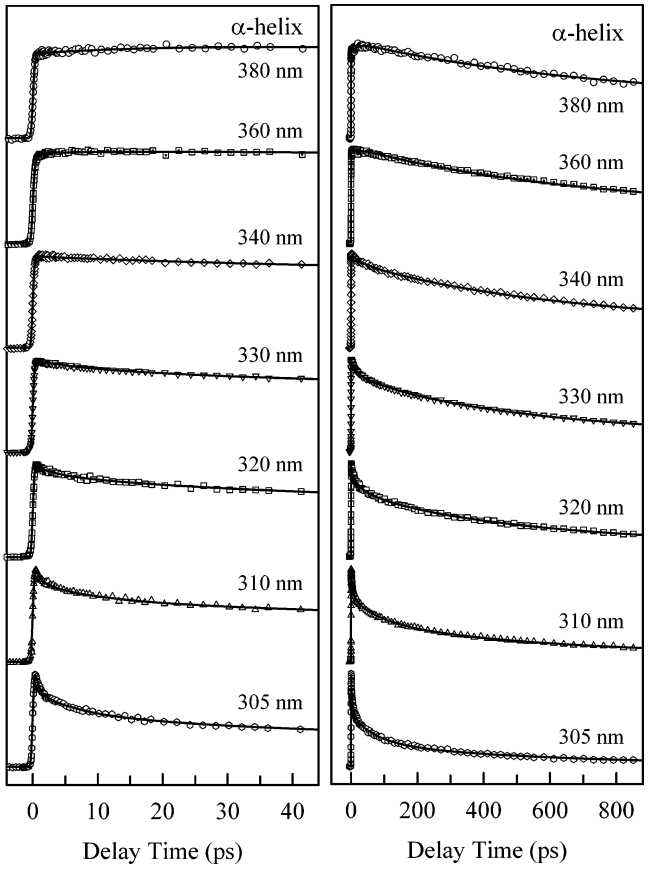

Figure 4. Normalized, fs-resolved fluorescence transients of a membrane-bound α-helical melittin in the short (left) and long (right) time ranges with a series of gated fluorescence emissions. Note that the solvation dynamics drastically slows down.

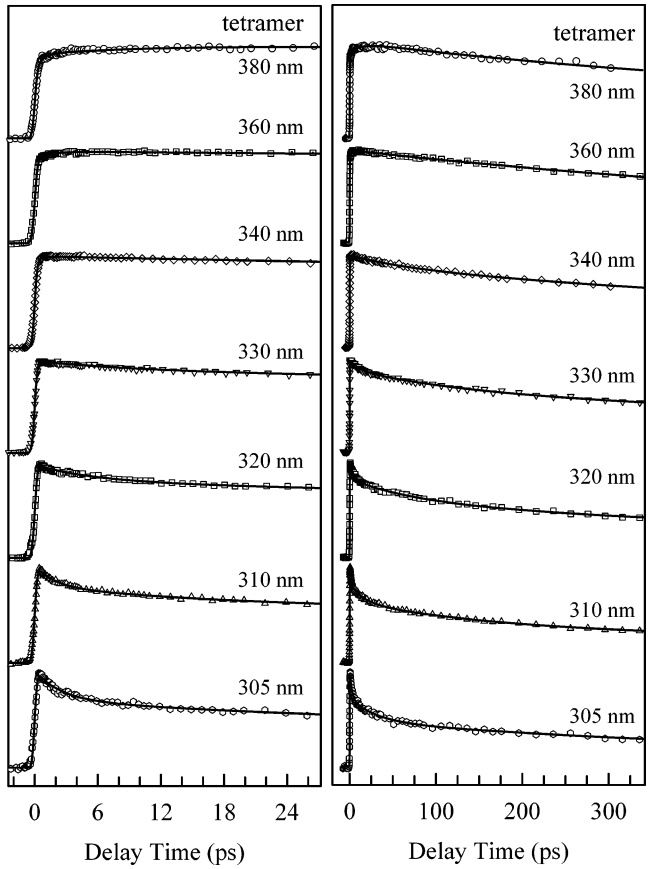

Figure 5. Normalized, fs-resolved fluorescence transients of a melittin tetramer formed in high-salt aqueous solution in the short (left) and long (right) time ranges with a series of gated fluorescence emissions. Note that the solvation dynamics is drastically slow, similar to that of melittin α-helix in Figure 4.

solvation at the blue side and the two solvation components decay in 2−10 and 30−100 ps. Clearly, no ultrafast decay components (<1 ps) were observed. At the red side (≥335 nm), we also observed two initial rise components in ∼0.5 and 5 ps.

B. Solvation Correlation Functions. The observed decay in the blue side and rise at the red side of wavelength-gated fluorescence transients is a typical signature of solvent relaxation. The overall fs-resolved emission spectrum (FRES) was constructed using eqs II.2 and II.3, and these results are shown in Figure 6 with several typical delay times. Similarly, the FRES due to the two lifetime emission mixture was also constructed (not shown). The overall emission maxima ν_s (Stokes shifts) and lifetime-associated emission maxima ν_l, derived from the log-normal fit of the corresponding FRES, are shown in Figure 7. Clearly, the solvation-complete time τ_{sc} and the corresponding emission maximum ν_{sc} are quite different from τ_{ss} and ν_{ss}. For example, in the random-coiled state of melittin the solvent relaxation completes in 140 ps while FRES takes 950 ps to reach its steady-state emission. In the additional 810 ps, the emission further shifts by 289 cm^{-1} ($\nu_{sc} - \nu_{ss}$). All derived emission maxima and times for different peptide conformations are summarized in Table 1.

We carefully considered the contributions of vibrational relaxation to the obtained total Stokes shifts by examining the change of FRES bandwidth with time. Typically, vibration relaxation results in bandwidth narrowing in emission spectra. We noticed that in the case of tryptophan the spectrum bandwidth of the two lifetime emissions (ν_l) also changes with time, for example, a total decrease of 200 cm^{-1} in 600 ps for the tetramer. However, we observed initial bandwidth broadening (not narrowing) of the total Stokes shift (ν_s) within several picoseconds in ∼100 cm^{-1} for tetramer, ∼300 cm^{-1} for α-helix, and ∼1500 cm^{-1} for random coil and KWK. These increases are mainly caused by the initial wave packet dynamics and the fitting procedures. Although W19 in three conformations has different water environments, the vibrational relaxation seems ultrafast within ∼1 ps, similar to the vibrational relaxation dynamics of tryptophan in bulk water.[52] This conclusion is also consistent with our obtained emission maxima of ∼320 nm at $t = 0$. The emission maxima of tryptophan in several proteins at temperature of 2 K at 300 nm excitation are about 320 nm.[53] In addition, our excitation of tryptophan at 290 nm is at the red edge of its absorption. Thus, the vibrational relaxation in our cases is ultrafast and probably minor, if any, and the observed total Stokes shifts dominantly result from the local solvation dynamics.

The solvation correlation functions were constructed using eq II.4, and the derived results are shown in Figure 8 and listed in Table 2. Clearly, solvation dynamics is drastically different for different peptide structures even with the same chemical identities. Specifically, for the tripeptide, the solvent response function can be represented by three exponential decays: 0.58 ps with 66% of total amplitude, 3.1 ps (27%), and 23 ps (7%). Free tryptophan in the same buffer gives a relaxation distribution of 0.52 ps (68%), 1.9 ps (23%), and 7.6 ps (9%). The first ultrafast component represents bulklike water motion. The slow solvation (3.1 and 23 ps) observed in tripeptide-KWK probably results from some rigid water molecules sticking to the positively charged lysine in close proximity of tryptophan.

In the random-coiled monomer, the solvation dynamics of W19 in melittin can be represented by two exponential decays:

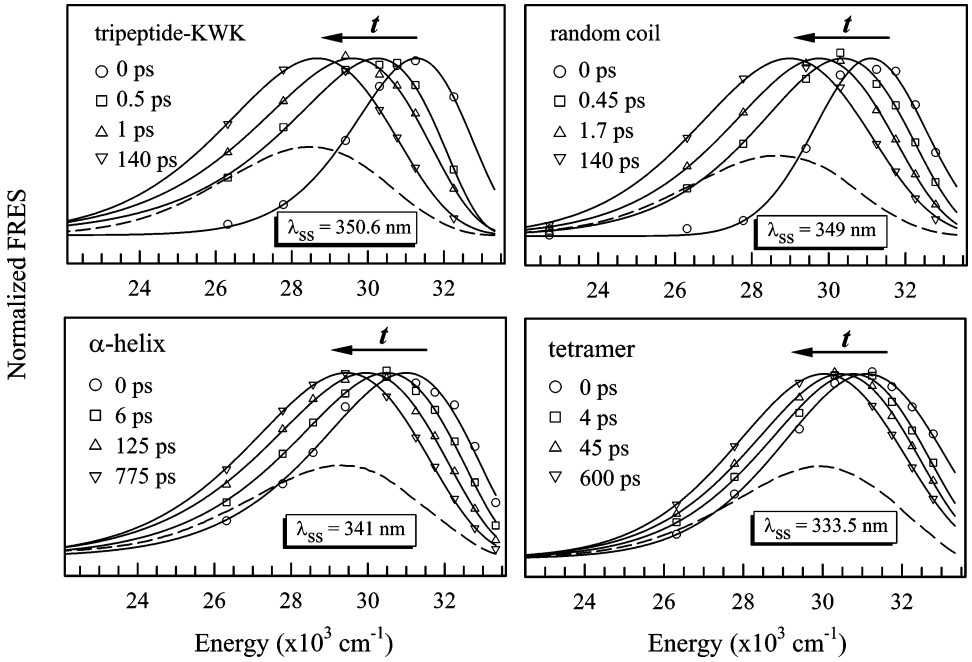

Figure 6. Representation of normalized overall FRES at several delay times, constructed from fs-resolved fluorescence transients (Figure 2−5) for tripeptide-KWK and melittin random coil, membrane-bound α-helix and tetramer. The dashed curves are the corresponding steady-state fluorescence emission spectra.

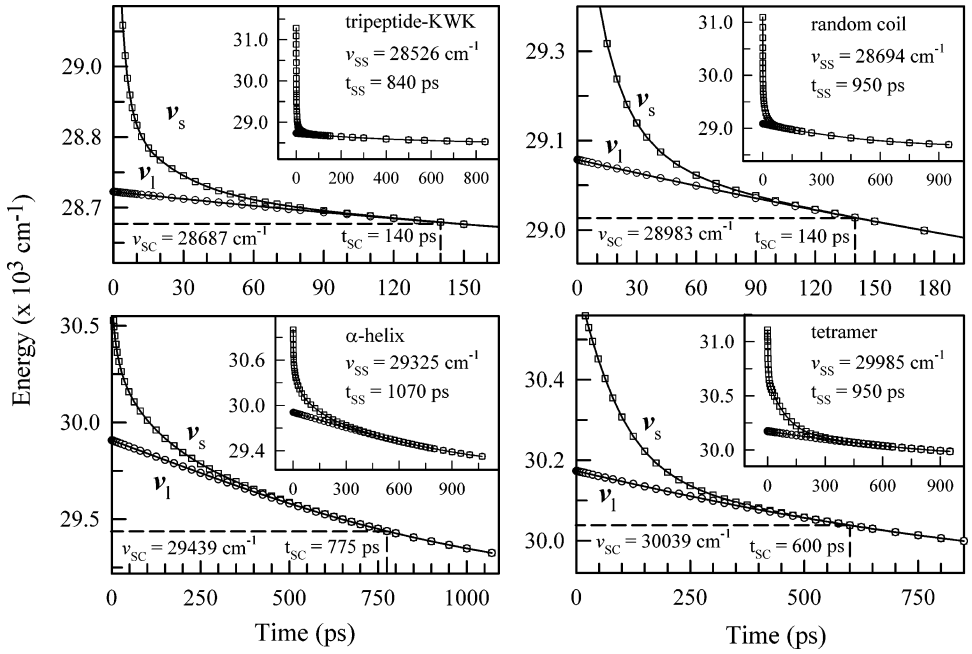

Figure 7. Femtosecond-resolved emission maxima of the overall emission spectra (ν_s) and the lifetime-associated emission spectra (ν_l) for all peptide conformations studied. The inset shows the entire evolution of ν_s and ν_l to reach the steady-state emission (ν_{ss}); see text.

TABLE 1: Emission Maxima and Time Constants from Construction of Time-Resolved Emissions[a]

	λ_0	λ_{sc}	τ_{sc}	λ_{ss}	τ_{ss}	λ_1	λ_2
tripeptide-KWK	319.70	348.70	140	350.6	840	332.70	351.10
melittin							
random coil	321.58	345.03	140	348.5	950	331.32	349.34
α-helix	322.55	339.69	775	341.0	1070	328.04	343.40
tetramer	321.48	332.90	600	333.5	950	326.80	334.47

[a] All emission maxima ($\lambda = 1/\nu$) and time constants (τ) are in units of nanometers and picoseconds, respectively.

0.62 ps (68%) and 14.7 ps (32%). The overall relaxation dynamics becomes slower than that of the tripeptide. In the membrane-bound α-helical structure, the relaxation process becomes drastically longer: 1.25 ps (35%), 14 ps (27%), and 114 ps (38%). The triple-exponential relaxation dynamics has been suggested resulting from three different types of water layers near membrane surfaces.[47,54,55] When the melittin monomer aggregates into a tetramer at high-salt concentration, the solvation dynamics also become much slower: 3 ps (47%) and 87 ps (53%). The tryptophan solvation in high-salt solution only takes about 10−20 ps;[56] thus the 87-ps solvation time must be related to the local tetramer conformation, which is discussed below.

C. Hydration Dynamics and Conformation Transitions. We observed distinct solvation dynamics of a 26 amino acid peptide in different conformations from a random coil, to an α-helix, and to a self-assembled tetramer. These observed

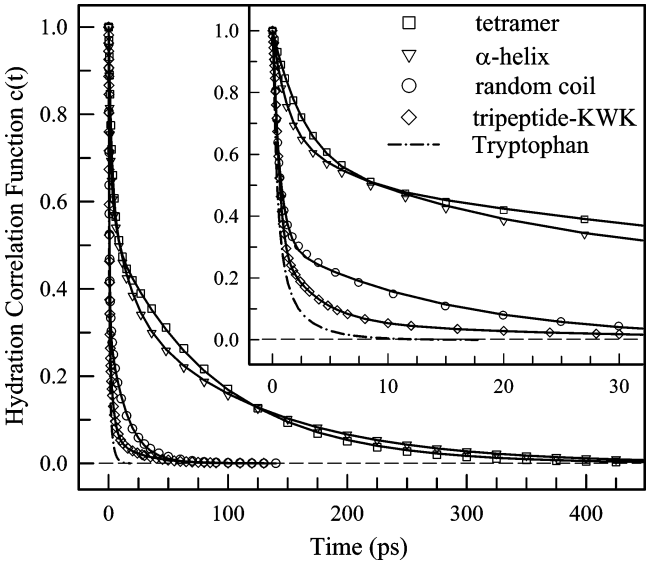

Figure 8. Hydration correlation functions probed by tryptophan in tripeptide-KWK and in three different conformations of melittin. The inset shows the correlation functions in the short time range. The solvation correlation function obtained for aqueous tryptophan is also shown for comparison.

different dynamics directly reflect the local ordering of water molecules and their motions mediating melittin conformational transitions.

(a) Hydration Dynamics and Protein Solvation. The constructed solvation correlation function is the response of the local environment around tryptophan to the sudden change of its static dipole moments from the ground state to the excited state. In principle, the response mainly results from both surrounding water molecules and neighboring protein residues (and backbone) besides a negligible contribution of ions in solution.[47,57] Although the motions of water molecules and their associated protein residues cannot be completely decoupled, certain rotational and translational motions of small water molecules may not give rise to significant local motions of the associated residues which are bulky and restricted by peptide structures.

TABLE 2: Results Obtained for Hydration Correlation Function $C(t)$ in Different Conformations[a]

	τ_1	β	τ_2	τ_3	c_1	c_2	c_3
tripeptide-KWK	0.58	1.35	3.1	23.3	0.66	0.27	0.07
melittin							
random coil	0.62	1	14.7		0.68	0.32	
α-helix	1.25	1	13.9	114	0.35	0.27	0.38
tetramer	3.01	1	87.0		0.47	0.53	

[a] All hydration correlation functions were best fitted with $c(t) = c_1 e^{-(t/\tau_1)^\beta} + c_2 e^{-t/\tau_2} + c_3 e^{-t/\tau_3}$ and $\Sigma_{i=1}^{3} c_i = 1$. The time constants are in units of picoseconds.

For all conformations studied here, we examined the local rigidity by measuring tryptophan anisotropy dynamics. These results are shown in Figure 9, and all initial decay in ~100 fs is due to internal conversion between ^1L_a and ^1L_b states.[47,52,58] Interestingly, we did not observe any local wobbling motion of tryptophan in tripeptide-KWK and the membrane-bound α-helical melittin. The time scale of 127 ps from the tripeptide represents the tumbling motion of the entire peptide in solution, indicating a rigid local structure probably caused by tryptophan-lysine(s) cation-π interactions.[59,60] Similarly, the anisotropy from the membrane-bound α-helical melittin is nearly constant, suggesting the tryptophan is located in a highly restricted environment in proximity of membrane headgroups, as depicted in Figure 1. For the random coil and tetramer, we observed a slow wobbling motion of tryptophan but at least three times slower than the corresponding solvation dynamics. Thus, the local side-chain motion, if any, takes a much longer time than the observed solvation dynamics. Also, the fluorescence emission maxima of tryptophan in all different conformations are well correlated with its hydration environments. As shown in Table 1, the emission peak of tryptophan shifts from ~350 to 333 nm for a full exposure to water in the tripeptide and random-coiled melittin to partial contact with water in the α-helical and tetramer melittin, respectively.

Thus, the observed solvation dynamics predominantly describes the hydration dynamics of local water molecules around tryptophan (peptides).

(b) Tryptophan Sensitivity and Local Hydration. The spatial resolution in hydration studies using tryptophan as a molecular

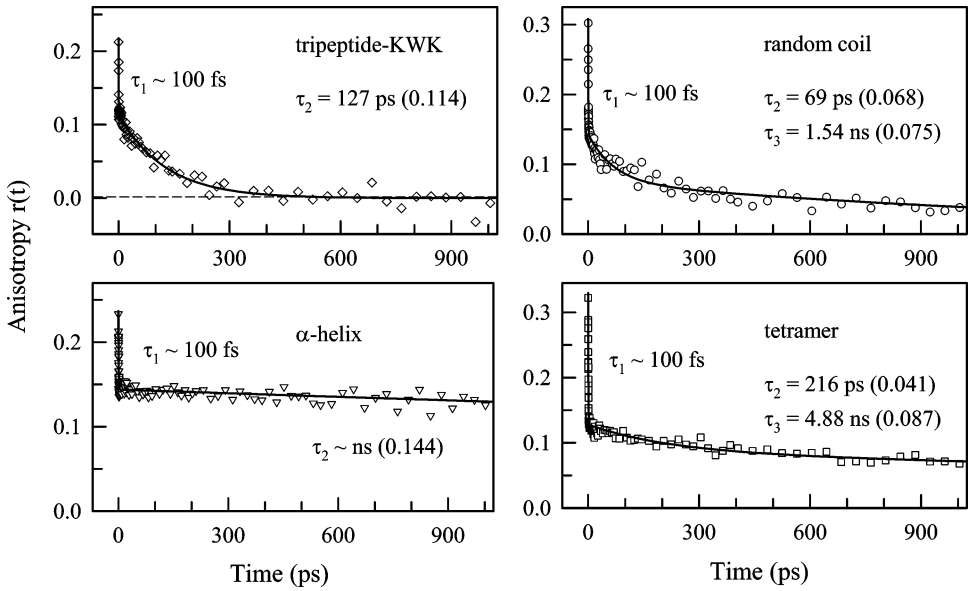

Figure 9. Time-resolved fluorescence anisotropy of tryptophan in tripeptide-KWK and in the different conformations of melittin. The initial ~100-fs decay results from the ultrafast internal conversion between ^1L_a and ^1L_b. Note that all observed rotational time constants are at least three times longer than the corresponding solvation dynamics.

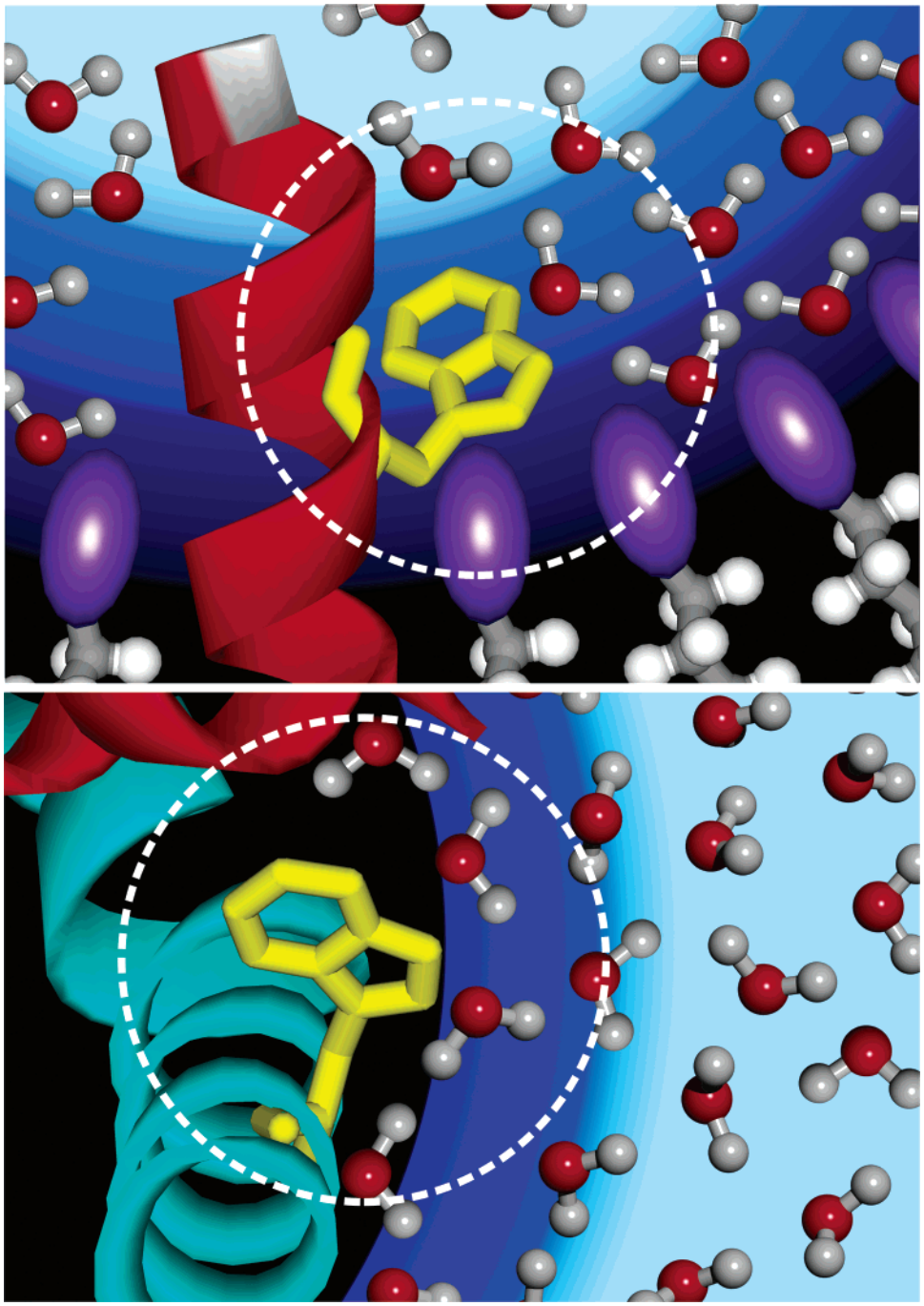

Figure 10. Schematic representation of the local-ordered water network/cluster in the α-helical melittin (upper) and melittin tetramer (lower). The probe sensitivity is indicated by the dashed circle in diameter of ∼7−10 Å. The blue color code represents different layers of water structures.

probe is determined by dipole−dipole interactions that follow a R^{-3} distance dependence. This method gives a better spatial resolution than using a distributed charge because of a R^{-1} distance dependence for the latter. Clearly, the definition of a hydration layer is sensitive to spatial and temporal resolutions intrinsic to the probing method. Care must be taken to provide the dynamical time scales without convolution of the intrinsic experimental factors.[1] Zewail et al. determined an ∼7 Å distance of the hydration layer,[46] consistent with the value determined by the scattering methods.[5] Friedrich et al.[61] suggested a distance of 4.5 Å for the interaction range of a molecular probe with its environment using a hole-burning method. The dipole−dipole interaction at ∼3.5 Å of the first solvent shell to the 7−10 Å solvent molecules drops to 12.5−4.3%. Therefore, using tryptophan we probe water in a distance up to ∼7−10 Å, that is, two to three layers of water molecules, which is also confirmed by recent theoretical calculations.[62] Figure 10 gives a schematic of local-ordered water network/clusters in the α-helical and tetramer melittin and the probing sensitivity of tryptophan.

(c) Solvent Relaxation and Local Polarization. The fluorescence emission maximum of tryptophan is often used to indicate its location in proteins through hydrophobicity of local environment. The steady-state Stokes shift, which is determined by the total local polarization, is an integration of the entire solvent relaxation and does not reflect the time scales of hydration. The hydration dynamics is the rate of hydrogen-bond breaking/making and is not necessary to reflect the magnitude of the Stokes shift. For example, we observed a similar long solvation dynamics (∼100 ps) of tryptophan in tetramer and in the membrane-bound α-helix, but the fluorescence emission maxi-

mum shifts from 334 nm for the former to 341 nm for the latter. Conversely, we observed a similar emission peak (~350 nm) for tryptophan in bulk water and in the random-coiled melittin, but the solvation dynamics occur in 1.6 and 14 ps, respectively (Figure 8). Thus, besides qualitatively knowing hydrophobicity of local environment through tryptophan emission maximum, the study of hydration dynamics is critical, and it not only provides the time scales of actual water motions but also elucidates the local ordering (structure) and rigidity of hydrogen-bonded water network/clusters. Revealing these interactions at the local molecular level is central to the understanding of protein stability and flexibility, as well as conformational transitions.

(d) Biological Water Motions and Peptide Conformational Transitions. Melittin in water is essentially a denatured protein with all constituting residues projecting into aqueous environment (Figure 1). The flexible W19 is fully exposed to water and probes the hydration dynamics occurring at a floppy random-coiled protein surface. The observed 620-fs component represents the ultrafast relaxation of bulklike water molecules including inertial/librational solvent motions while the 14.7-ps dynamics arises from the relaxation of local-ordered biological water. This longer water relaxation is similar to the reported surface hydration dynamics of proteins.[46] Thus, the observed time scale of 10−20 ps reflects the fluctuating nature of the ordered water surrounding the surface of denatured melittin.

Melittin readily binds to membranes and performs toxic function of membrane lysis. The first twenty mainly hydrophobic residues strongly interact with lipids. The last six hydrophilic residues protrude into interfacial water layers. Melittin was also observed to form an α-helical structure in alcohol solvent.[25−27] It is believed that the aliphatic chain of alcohol reduces the hydrogen bonding between amide protons and surrounding solvent molecules, promotes the intramolecular hydrogen bonding in melittin, and stabilizes the secondary α-helical structure.[34] Thus, the mobile water molecules as observed in the random coil disfavor the α-helical formation in solution. In the membrane−water interface, water is much more rigid and ordered. The immobilized water promotes the secondary α-helical formation at least in the C-terminus. We observed three distinct time scales of 114, 15, and 1.25 ps, representing three different types of water structures near the membrane interface: well-ordered, quasi-free, and bulklike.[47] The longest 114-ps water dynamics represents the slow interfacial water motion, stabilizing the structures of the α-helix and lipid.

The X-ray crystallographic structure of melittin in membrane has not yet been resolved, but extensive studies have shown that the membrane-bound melittin adopts an amphipathic α-helix.[18−21] Whether the peptide would lie down at the membrane surface or insert into the membrane highly depends on many factors such as temperature, surface curvature, and chemical identity of headgroups. For a neutral headgroup lipid and at ambient temperature, it is believed that melittin partially inserts into the membrane, as also confirmed by recent molecular dynamics (MD) simulations.[37] Compared with the solvation dynamics obtained from free tryptophan in the lipidic cubic phase water channel (108, 9.2, and 0.56 ps), the tryptophan in the α-helix probes less bulklike water, and thus it is closer to the membrane, consistent with the fluorescence emission peaks shifting from 344 nm for free tryptophan in the water channel to 341 nm for the membrane-bound α-helix.

The emission peak at 341 nm is similar to that of typical surface tryptophan emission of proteins and also rules out the possibility of a buried W19 inside the hydrophobic core underneath polar headgroups. Our anisotropic studies (Figure 9) showed a highly restricted local motion, indicating that W19 locates at the interface around headgroups and well-ordered water molecules. Also, tryptophan side chains in most membrane proteins have been observed to reside preferentially at membrane interfaces most likely due to their flat rigid shape and π-electronic structure (aromaticity).[63,64] All these facts support that the α-helix penetrates into the membrane until W19 is spatially hindered by the interfacial polar headgroups (Figure 1). We are also aware of the fact that W19 and ordered water could penetrate into the membrane at certain lipidic conditions (Figure 10).

The observed hydration dynamics here is significant and reflects local water ordering (structure) and its motion in the membrane nanochannel of 50 Å in diameter. The ordered water near the channel wall fluctuates in ~100 ps, significantly longer than water relaxation in bulk and at protein surfaces. Thus, the time scale of ~100 ps is necessary to keep the global structural stability of lipid bilayers as well as the protein structural integrity of the α-helical content in membrane-bound melittin.

At high ionic strength, ions are solvated by water molecules and such processes reduce the availability of water molecules interacting with melittin, enhancing the formation of α-helical content. Due to the unique sequence and structural integrity, a large hydrophobic surface is formed in the α-helical monomer (and dimer), driving tetramerization to form a large hydrophobic core in the center of the tetramer. Four highly charged C-terminals form two crossing joints (Figure 1), and each of these two regions has eight positively charged residues. Besides the salt dielectric screening of the interchain electrostatic repulsion, water molecules solvate these charged residues and associated ions and form a highly ordered structure around two assembled regions, therefore stabilizing the local tetramer structures. The longer water relaxation observed here takes 87 ps, significantly longer than the surface hydration dynamics of most proteins which have been studied so far.[46,65] This time scale of ~87 ps, similar to ordered-water motion observed in membrane interfaces, again reflects the importance of appropriate water mobility for the self-assembly of both lipid bilayers and high-order structures of melittin.

IV. Conclusion

In this article, we reported our systematic studies of hydration dynamics in different conformations of melittin from a random coil, to a folded α-helix, and to a self-assembled tetramer using intrinsic tryptophan as a molecular probe. With femtosecond resolution, we observed the solvation dynamics with two time scales of 0.62 ps (68%) and 14.7 ps (32%) in a random-coiled monomer. The former ultrafast component mainly represents inertial/librational solvation dynamics of bulklike water molecules, and the latter, slower one reflects surface-type hydration dynamics of proteins, indicating that a hydrogen-bonded water network/cluster was formed. As a comparison, we also studied a tripeptide (KWK) and basically bulklike water solvation was observed, lacking significant ordered-water formation. In lipidic aqueous solution, melittin folds into a secondary α-helical structure at membrane−water interfaces, and we observed hydration dynamics with three distinct time scales: 1.25 ps (35%), 13.9 ps (27%), and 114 ps (38%), implying three different layers of water structures in the water nanochannel (50 Å in diameter). The slowest dynamics represents the interfacial water motion of a well-ordered water structure along the membrane surface.

In high-salt aqueous solution, the salt dielectric screening and ionic solvation promote the hydrophobic core collapse in melittin

aggregation and facilitate the tetramer formation. This tertiary structure is further stabilized by the strong hydrophilic interactions of charged residues and associated ions with hydrogen-bonded water molecules in the two assembled regions. The hydration dynamics was observed to occur in 3 ps (47%) and 87 ps (53%), significantly slower than water relaxation at protein surfaces but similar to water motion at membrane interfaces. Thus, the observed time scale of ~100 ps represents a type of necessarily dynamical ordering of water molecules to mediate high-order structure formation of melittin in the α-helix and self-assembled tetramer. These studies elucidate a critical role of a dynamically ordered water network/cluster on the picosecond time scales in promoting peptide conformational transitions as well as maintaining protein structural stability, flexibility, and integrity.

Acknowledgment. This work was supported by the Selective Investment of The Ohio State University through the Biophysics Initiative in the Physics department, the Petroleum Research Fund (PRF-42734-G4), and the NSF (CHE-0517334). We like to thank Professors Ahmed H. Zewail (Caltech), Sherwin Singer (OSU), and Mr. Ali Hassanali for many stimulating discussions. Also, thanks to Dr. Kenneth Riedl (Professor Martin Caffrey's group) for his preparation of the lipidic cubic phase sample and Jeff Stevens for his thorough reading of the manuscript.

Supporting Information Available: All fitting parameters of amplitudes and time constants for transients in Figures 2−5. This material is available free of charge via the Internet at http://pubs.acs.org.

References and Notes

(1) Pal, S. K.; Zewail, A. H. *Chem. Rev.* **2004**, *104*, 2099. Pal, S. K.; Peon, J.; Bagchi, B.; Zewail, A. H. *J. Phys. Chem. B* **2002**, *106*, 12376.
(2) Wüthrich, K. *Angew. Chem., Int. Ed.* **2003**, *42*, 3340.
(3) Mattos, C. *Trends Biochem. Sci.* **2002**, *27*, 203.
(4) Bizzarri, A. R.; Cannistraro, S. *J. Phys. Chem. B* **2002**, *106*, 6617.
(5) Finney, J. L. *Faraday Discuss.* **1996**, *103*, 1. See references therein.
(6) Bryant, R. G. *Annu. Rev. Biophys. Biomol. Struct*. **1996**, *25*, 29.
(7) *Protein−Solvent Interactions*; Gregory, R. B., Ed.; Marcel Dekker: New York, 1995.
(8) Timasheff, S. N. *Annu. Rev. Biophys. Biomol. Struct.* **1993**, *22*, 67.
(9) Teeter, M. M. *Annu. Rev. Biophys. Biophys. Chem.* **1991**, *20*, 577.
(10) Otting, G.; Liepinsh, E.; Wüthrich, K. *Science* **1991**, *254*, 974.
(11) Fernández-Escamilla, A. M.; Cheung, M. S.; Vega, M. C.; Wilmanns, M.; Onuchic, J. N.; Serrano, L. *Proc. Natl. Acad. Sci. U.S.A.* **2004**, *101*, 2834.
(12) Rhee, Y. M.; Sorin, E. J.; Jayachandran, G.; Lindahl, E.; Pande, V. S. *Proc. Natl. Acad. Sci. U.S.A.* **2004**, *101*, 6546.
(13) Fändrich, M.; Fletcher, M. A.; Dobson, C. M. *Nature* **2001**, *410*, 165.
(14) Fändrich, M.; Forge, V.; Buder, K.; Kittler, M.; Dobson. C. M.; Diekmann, S. *Proc. Natl. Acad. Sci. U.S.A.* **2003**, *100*, 15463.
(15) Fenimore, P. W.; Frauenfelder, H.; McMahon, B. H.; Parak, F. G. *Proc. Natl. Acad. Sci. U.S.A.* **2002**, *99*, 16047. Frauenfelder, H.; Fenimore, P. W.; McMahon, B. H. *Biophys. Chem.* **2002**, *98*, 35.
(16) Purkiss, A.; Skoulaikis, S.; Goodfellow, J. M. *Philos. Trans. R. Soc. London, Ser. A* **2001**, *359*, 1515.
(17) Straub, J. E.; Guevara, J.; Huo, S. H.; Lee, J. P. *Acc. Chem. Res.* **2002**, *35*, 473. Massi, F.; Straub, J. E. *Biophys. J.* **2001**, *81*, 697.
(18) Ohki, S.; Marcus, E.; Sukumaran, D. K.; Arnold, K. *Biochim. Biophys. Acta* **1994**, *1194*, 223.
(19) Frey, S.; Tamm, L. K. *Biophys. J.* **1991**, *60*, 922.
(20) Dempsey, C. E. *Biochim. Biophys. Acta* **1990**, *1031*, 143.
(21) Vogel, H.; Jahnig, F. *Biophys. J.* **1986**, *50*, 573.
(22) Goto, Y.; Hagihara, Y. *Biochemistry* **1992**, *31*, 732.
(23) Quay, S. C.; Condie, C. C. *Biochemistry* **1983**, *22*, 695.
(24) Bello, J.; Bello, H. R.; Granados, E. *Biochemistry* **1982**, *21*, 461.
(25) Gerig, J. T. *Biophys. J.* **2004**, *86*, 3166.
(26) Kemple, M. D.; Buckley, P.; Yuan, P.; Prendergast, F. G. *Biochemistry* **1997**, *36*, 1678.
(27) Lakowicz, J. R.; Gryczynski, I.; Wiczk, W.; Laczko, G.; Prendergast, F. C.; Johnson, M. L. *Biophys. Chem.* **1990**, *36*, 99.
(28) Raghuraman, H.; Chattopadhyay, A. *Biophys. J.* **2004**, *87*, 2419.
(29) Yuan, P.; Fisher, P. J.; Prendergast, F. G.; Kemple, M. D. *Biophys. J.* **1996**, *70*, 2223.
(30) Okada, A.; Wakamatsu, K.; Miyazawa, T.; Higashijima, T. *Biochemistry* **1994**, *33*, 9438.
(31) Iwadate, M.; Asakura, T.; Williamson, M. P. *Eur. J. Biochem.* **1998**, *257*, 479.
(32) Wilcox, W.; Eisenberg, D. *Protein Sci.* **1992**, *1*, 641.
(33) Terwilliger, T. C.; Eisenberg, D. *J. Biol. Chem.* **1982**, *257*, 6010. Terwilliger, T. C.; Eisenberg. D. *J. Biol. Chem.* **1982**, *257*, 6016.
(34) Liu, H. L.; Hsu, C. M. *Chem. Phys. Lett.* **2003**, *375*, 119.
(35) Roccatano, D.; Colombo, G.; Fioroni, M.; Mark, A. E. *Proc. Natl. Acad. Sci. U.S.A.* **2002**, *99*, 12179.
(36) Lin, J. H.; Baumgaertner, A. *Biophys. J.* **2000**, *78*, 1714.
(37) Bachar, M.; Becher, O. M. *J. Chem. Phys.* **1999**, *111*, 8672.
(38) Cheng, Y. K.; Rossky, P. J. *Nature* **1998**, *392*, 696. Cheng, Y. K.; Sheu, W. S.; Rossky, P. J. *Biophys. J.* **1999**, *76*, 1734.
(39) Raghuraman, H.; Chattopadhyay, A. *Langmuir* **2003**, *19*, 10332. Chattopadhyay, A.; Rukmini, R. *FEBS Lett.* **1993**, *335*, 341.
(40) Ladokhin, A. S.; Jayasinghe, S.; White, S. H. *Anal. Biochem.* **2000**, *285*, 235.
(41) Tran, C. D.; Beddard, G. S. *Eur. J. Biophys.* **1985**, *13*, 59.
(42) Pandit, A.; Larson, O. F.; van Stokkum, I. H. M.; van Grondelle, R.; Kraayenhof, R.; van Amerongen, H. *J. Phys. Chem. B* **2003**, *107*, 3086.
(43) Hansen, J. E.; Rosenthal, S. J.; Fleming, G. R. *J. Phys. Chem.* **1992**, *96*, 3034.
(44) John, E.; Jahnig, F. *Biophys. J.* **1988**, *54*, 817.
(45) Vogel, H.; Rigler, R. In *Structure, Dynamics and Function of Biomolecules*; Ehrenberg, A., Rigler, R., Gräslund, A., Nilsson, L., Eds.; Springer-Verlag: Berlin, Germany, 1987.
(46) Pal, S. K.; Peon, J.; Zewail, A. H. *Proc. Natl. Acad. Sci. U.S.A.* **2002**, *99*, 1763. Peon, J.; Pal, S. K.; Zewail, A. H. *Proc. Natl. Acad. Sci. U.S.A.* **2002**, *99*, 10964. Zhao, L.; Pal, S. K.; Xia, T.; Zewail, A. H. *Angew. Chem., Int. Ed.* **2004**, *43*, 60.
(47) Lu, W.; Kim, J.; Qiu, W.; Zhong, D. *Chem. Phys. Lett.* **2004**, *388*, 120.
(48) Lu, W.; Qiu, W.; Kim, J.; Okobiah, O.; Hu, H.; Gokel, G. W.; Zhong, D. *Chem. Phys. Lett.* **2004**, *394*, 415.
(49) Saxena, C.; Sancar, A.; Zhong, D. *J. Phys. Chem. B* **2004**, *108*, 18026.
(50) Cherezov, V.; Clogston, J.; Misquitta, Y.; Abdel-Gawad, W.; Caffrey, M. *Biophys. J.* **2002**, *83*, 3393. Caffrey, M. *J. Struct. Biol.* **2003**, *142*, 108.
(51) Maroncelli, M.; Fleming, G. R. *J. Chem. Phys.* **1987**, *86*, 6221. Horng, M. L.; Gardecki, J.; Papazyan, A.; Maroncelli, M. *J. Phys. Chem.* **1995**, *99*, 17311.
(52) Zhong, D.; Pal, S. K.; Zhang, D.; Chan, S. I.; Zewail, A. H. *Proc. Natl. Acad. Sci. U.S.A.* **2002**, *99*, 13.
(53) Scott, T. W.; Campbell, B. F.; Cone, R. L.; Friedman, J. M. *Chem. Phys.* **1989**, *131*, 63.
(54) Willard, D. M.; Riter, R. E.; Levinger, N. E. *J. Am. Chem. Soc.* **1998**, *120*, 4151.
(55) Finer, E. G. *J. Chem. Soc., Faraday Trans.* **1973**, *69*, 1590.
(56) Lu, W.; Zhong, D. In preparation.
(57) Faeder, J.; Ladanyi, B. M. *J. Phys. Chem. B* **2005**, *109*, 6732.
(58) Shen, X. H.; Knutson, J. R. *J. Phys. Chem. B* **2001**, *105*, 6260.
(59) Dougherty, D. A. *Science* **1996**, *271*, 163. Ma, J. C.; Dougherty, D. A. *Chem. Rev.* **1997**, *97*, 1303.
(60) Meyer, E. A.; Castellano, R. K.; Diederich, F. *Angew. Chem., Int. Ed.* **2003**, *42*, 1210.
(61) Lesch, H.; Schlichter, J.; Friedrich, J.; Vanderkooi, J. M. *Biophys. J.* **2004**, *86*, 467.
(62) Vivian, J. T.; Callis, P. R. *Biophys. J.* **2001**, *80*, 2093.
(63) Durell, S. R.; Guy, H. R. *Biophys. J.* **1992**, *62*, 238. Bogusz, S.; Boxer, A.; Busath, D. D. *Protein Eng.* **1992**, *5*, 285. Doyle, D. A.; Cabral, J. M.; Pfuetzner, R. A.; Kuo, A. L.; Gulbis, J. M.; Cohen, S. L.; Chait, B. T.; MacKinnon, R. *Science* **1998**, *280*, 69.
(64) Yau, W.-M.; Wimley, W. C.; Gawrisch, K.; White, S. H. *Biochemistry* **1998**, *37*, 14713.
(65) Kao, Y.-T.; Zhong, D. In preparation.